

# Comparative Positron-Emission Tomography (PET) Imaging and Phototherapeutic Potential of $^{124}\text{I}$ -Labeled Methyl- 3-(1'-iodobenzoyloxyethyl)pyropheophorbide-*a* vs the Corresponding Glucose and Galactose Conjugates

Suresh K. Pandey,<sup>†</sup> Munawwar Sajjad,<sup>\*,‡</sup> Yihui Chen,<sup>†</sup> Xiang Zheng,<sup>†</sup> Rutao Yao,<sup>‡</sup> Joseph R. Missert,<sup>†</sup> Carrie Batt,<sup>†</sup> Hani A. Nabi,<sup>‡</sup> Allan R. Oseroff,<sup>§</sup> and Ravindra K. Pandey<sup>\*,†</sup>

PDT Center and Department of Dermatology, Roswell Park Cancer Institute, Buffalo, New York 14263, and Department of Nuclear Medicine, State University of New York, Buffalo, New York 14214

Received September 26, 2008

In our present study, 3-(1'-*m*-iodobenzoyloxyethyl)pyropheophorbide-*a* methyl ester **1**, 3-(1'-*m*-iodobenzoyloxyethyl)-17<sup>2</sup>-{(2-deoxy)glucose}pyropheophorbide-*a* **2**, and 3-(1'-*m*-iodobenzoyloxyethyl)-17<sup>2</sup>-{(1-deoxy)-galactose}pyropheophorbide-*a* **3** were synthesized and converted into the corresponding  $^{124}\text{I}$ -labeled analogues by reacting the intermediate trimethyltin analogues with  $\text{Na}^{124}\text{I}$ . Photosensitizers **1–3** were evaluated for the PDT efficacy in C3H mice bearing RIF tumors at variable doses and showed a significant long-term tumor cure. Among the compounds investigated, the non-carbohydrate analogue **1** was most effective. These results were in contrast to the *in vitro* data, where compared to the parent analogue the corresponding galactose and glucose derivatives showed enhanced cell kill. Among the corresponding  $^{124}\text{I}$ -labeled analogues, excellent tumor images were obtained from compound **1** in both tumor models (RIF and Colon-26) and the best tumor contrast was observed at 72 h after injection. Conjugating a glucose moiety to photosensitizer **1** initially diminished its tumor uptake, whereas with time the corresponding galactose analogue showed improved tumor contrast.

## Introduction

Molecular imaging is a newly emerging field in which the modern tools of molecular and cell biology are being combined together to the state-of-art technology for noninvasive imaging. The goals of this field are to develop technologies for studying biological processes as well as to detect and monitor various diseases including cancer. Molecular imaging has its roots in nuclear medicine and in many ways is a direct extension of this existing discipline.<sup>1</sup> In recent years, positron-emission tomography (PET), a noninvasive imaging technique that exploits the unique decay physics of positron-emitting isotopes, has created enormous interest in tumor imaging in order to provide a functional or metabolic assessment of normal tissues or disease conditions.<sup>2,3</sup> PET with  $^{18}\text{F}$ -FDG is approved by the Center for Medicare and Medicaid Services for diagnosing, staging, and restaging lung cancer, colorectal cancer, lymphoma, melanoma, head and neck cancer, and esophageal cancer. Although  $^{18}\text{F}$ -FDG is an exquisite tumor-localizing tracer, it is not tumor-specific. The uptake of  $^{18}\text{F}$ -FDG reflects glucose use in essentially any tissue; its increased uptake in tumors is a result of increased and inefficient use of glucose. Other benign processes associated with cells that have increased glucose use, such as inflammatory cells or hyperplastic bone marrow or thymic cells, also have enhanced  $^{18}\text{F}$ -FDG uptake. Thus, increased  $^{18}\text{F}$ -FDG uptake is usually observed in infectious and inflammatory processes, inflammatory changes after surgery or irradiation, and thymic or bone marrow hyperplasia after treatment. Additionally, the short half-life of  $^{18}\text{F}$ -isotope (110

min) limits its use in studies involving antibodies and in photodynamic therapy (PDT), where the photosensitizers often take a considerably longer time to both accumulate in tumors and clear from the nontargeted organs.<sup>4</sup> In this respect,  $^{124}\text{I}$  is a better choice because of its half-life of 4.2 days and because it enables longitudinal imaging studies using animal PET. The labeling technique for  $^{124}\text{I}$ -isotope is now well established, and this approach is continuously being used in labeling a variety of biologically active molecules.<sup>5</sup>

For quite some time our laboratory has been investigating the utility of porphyrin-based compounds for the use in photodynamic therapy (PDT), which is now a well-established noninvasive modality for tumor treatment.<sup>6</sup> A purified form of the hematoporphyrin derivative, developed in our Institute by Dougherty and co-workers, has been approved worldwide for the treatment of various cancers and is being marketed by Axcan Pharmaceuticals, Canada.<sup>7</sup> One of the drawbacks of the hematoporphyrin derivative has been its skin phototoxicity; the patients are advised to be away from direct sunlight for 6–8 weeks after the treatment. Therefore, efforts are underway in various laboratories to develop a photosensitizer at least as effective as the purified form of the hematoporphyrin derivative but with reduced skin phototoxicity. At the PDT Center of our Institute, HPPH, a compound derived from chlorophyll-*a*, has shown promising results with limited skin phototoxicity, and it is currently in phase I/II clinical trials.<sup>8</sup> Efforts are currently underway in our and other laboratories to develop target-specific agents by conjugating the porphyrin-based compounds to target-specific moieties for binding to those proteins known for their overexpression in tumor cells.<sup>9</sup>

For optimizing the PDT treatment by a “see and treat approach”, we have been exploring the utility of tumor-avid photosensitizers as vehicles to deliver the desired imaging moiety to tumors. We have previously reported the advantages of this approach in developing certain HPPH–cyanine dyes and

\* To whom correspondence should be addressed. For R.K.P.: phone, 716-845-3203; fax, 716-845-8920; e-mail, ravindra.pandey@roswellpark.org. For M.S.: phone, 716-838-5889, extension 118; fax, 716-838-4918; e-mail, msajjad@buffalo.edu.

<sup>†</sup> PDT Center, Roswell Park Cancer Institute.

<sup>‡</sup> State University of New York.

<sup>§</sup> Department of Dermatology, Roswell Park Cancer Institute.

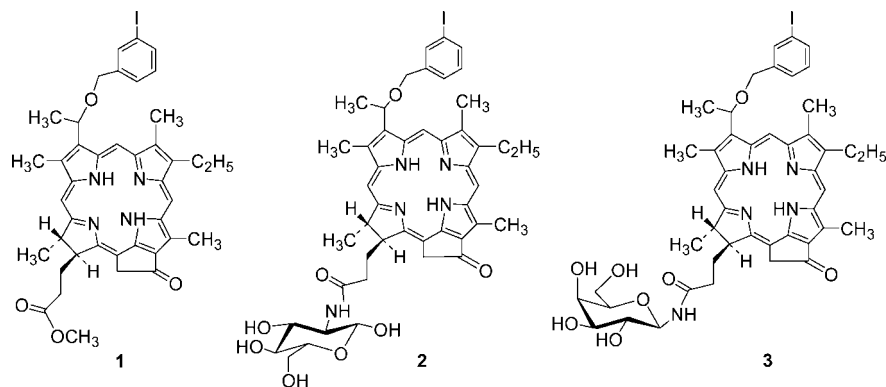


**Figure 1.** Chemical structures of the lead compound **1** and its corresponding glucose **2** and galactose **3** conjugates.

HPPH–DTPA conjugates for PDT/fluorescence imaging and PDT/MR imaging, respectively.<sup>10</sup> However, fluorescence imaging (planer imaging) has limited applications for imaging deeply seated tumors because of the relatively low tissue penetration ability of the visible light,<sup>10</sup> whereas the MR imaging suffers from low sensitivity at the molecular target level. In contrast, nuclear imaging, e.g., PET and single photon emission computer tomography (SPECT), has been widely used for human tomographic imaging as a result of using high energy photons and is intrinsically suited for molecular imaging. Therefore, we have been interested in using certain tumor-avid porphyrin-based molecules as vehicles to deliver the desired nuclide to the target-site for nuclear imaging.<sup>11</sup> In our earlier study, as a proof of principle approach, we introduced <sup>124</sup>I nuclide in methylpyropheophorbide-*a*, and this compound showed its potential in both tumor imaging and phototherapy in mice (C3H) bearing RIF tumors.<sup>12</sup>

It has been reported by various investigators that introduction of glucose and  $\beta$ -galactose moieties in photosensitizers<sup>13</sup> leads to increased efficiency in tumor uptake. It is believed that <sup>18</sup>F-FDG, an analogue of glucose, enters cells via glucose transporters (GLUT). Speizer explored the utility of glucose by incorporating it into a fluorescent molecule into human erythrocytes, and this approach was then extended in developing other analogues.<sup>14</sup> In a similar approach, recently, a pyropheophorbide-2-deoxyglucosamide has been reported as a new photosensitizer targeting the glucose transporters,<sup>15</sup> and it is proposed to be trapped in tumor cells via the GLUT/hexokinase pathway.

To investigate the utility of the carbohydrate moieties in developing target-specific photosensitizers, we conjugated a highly effective photosensitizer (HPPH, a chlorophyll derivative) with a series of carbohydrates, and among all the compounds, the HPPH– $\beta$ -galactose conjugate produced higher photosensitizing efficacy than HPPH in mice bearing RIF tumors.<sup>16</sup> On the basis of these findings, we hypothesized that compared to compound **1**, the corresponding glucose **2** and galactose **3** analogues (Figure 1) should produce improved PET imaging and PDT efficacy. The comparative *in vivo* imaging, biodistribution, and therapeutic potential of these compounds were investigated in BALB/c mice bearing Colon-26 tumors.

## Results and Discussion

**Chemistry and Radiochemistry.** In a sequence of reactions, compound **1** was synthesized from methyl pheophorbide-*a*,<sup>17</sup> which in turn was isolated from *Spirulina pacifica* by following the methodology developed by Smith et al.<sup>18</sup> The methyl ester functionality present at position-17<sup>2</sup> was then hydrolyzed with aqueous LiOH in an inert atmosphere to yield the corresponding carboxylic acid **4**. The activated succinimido derivative **5** was

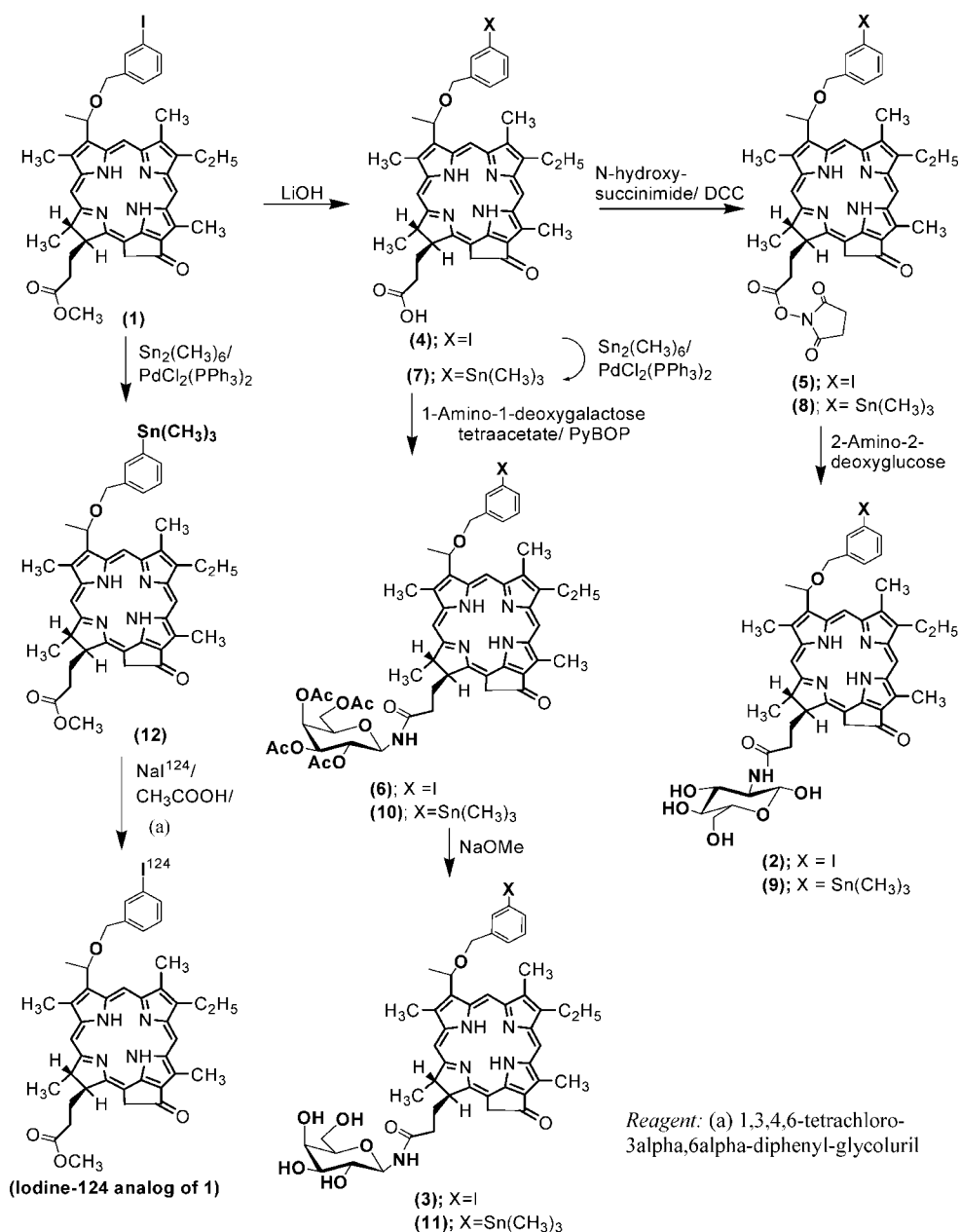
reacted with 2-amino-2-deoxyglucose, and compound **2** was obtained in 56% overall yield. By use of a similar approach, compound **4** was also condensed with 1-amino-1-deoxygalactose tetraacetate in the presence of (benzotriazol-1-yloxy)tripyrrolidinophosphonium hexafluorophosphate (PyBOP) to produce intermediate **6**, which upon standard acetyl deprotection by treatment with sodium methoxide afforded the corresponding galactose conjugate **3** in 48% yield (Scheme 1).

For labeling the glucose **2** and the galactose **3** conjugates radiospecifically with iodine-124, trimethylstannyl derivatives **9** and **11** were synthesized from **1** by following the reaction sequences illustrated in Scheme 1. In brief, compound **4**, obtained by aqueous LiOH hydrolysis of **1**, upon reacting with hexamethylditin gave the corresponding trimethylstannyl analogue **7**, which was converted to the corresponding succinimido derivative **8**. Further reaction of **8** with 2-amino-2-deoxyglucose produced the trimethylstannyl derivative **9** in 68% yield. For the preparation of **11**, the trimethylstannyl derivative **7** was directly reacted with 1-amino-1-deoxygalactose tetraacetate in the presence of PyBOP and gave the acetylated galactose conjugate **10** in 55% yield. The deprotection of the acetoxy groups on treatment with sodium methoxide afforded the desired galactose analogue **11** in modest yield. All final compounds were analyzed by HPLC for chemical purity (retention times for the glucose **2** and galactose **3** conjugates were 8.17 and 8.02 min, respectively (for details, see the Experimental Section). Conjugation of 2-deoxyglucose and 1-deoxygalactose with the lead compound **1** at 17<sup>2</sup>-position produced the corresponding conjugates **2** and **3** having identical molecular weight and lipophilicity but with a significant difference in the HPLC retention times (see Supporting Information).

For <sup>124</sup>I-labeling, trimethylstannyl derivatives **9**, **11**, and **12** were separately reacted for 15 min at room temperature with Na<sup>124</sup>I (produced in UB cyclotron facility<sup>19</sup> in the presence of 1,3,4,6-tetrachloro-3 $\alpha$ ,6 $\alpha$ -diphenylglucuril. After 15 min the bead was removed and the radioactive reaction mixture was purified by HPLC. The peaks corresponding to the desired iodinated products **1**–**3** were collected, and the <sup>124</sup>I-labeling was confirmed by RadioTLC.

### Comparative Biodistribution of <sup>124</sup>I Labeled Pyropheophorbide-*a* (**1**) and Its Glucose (**2**) and Galactose (**3**) Derivatives.

Four C3H mice were implanted with RIF tumors over the right shoulder. With this tumor location, mice could be restrained in a Plexiglas holder and PDT could be performed without using any anesthesia procedure. Figure 2 shows the *in vivo* biodistribution results in terms of percent injected dose per unit weight (% ID/g) for the three compounds at 24, 48, 72, and 96 h postinjection. Among the three compounds, compound **1** had the highest tumor uptake value at 24 and 48 h time points,

**Scheme 1.** Synthetic Strategy for the Preparation of Glucose and Galactose Conjugates (**2** and **3**, Respectively) from **1** and the Corresponding  $^{124}\text{I}$ -Labeled Analogues

topping at 4.1% ID/g at the 24 h postinjection. Compound **3**, the galactose derivative of compound **1**, was found to have higher uptake values at the 72 and 96 h time points; however, it also had considerably higher liver and spleen uptake at all time points. Compound **2**, the glucose analogue of compound **1**, had the least tumor uptake among all compounds at all time points, and it also had lower spleen and liver uptake than **3** but higher than that of **1**. The corresponding animal PET images showed clearly the tumor site with **1** at time points 24 h after injection, indicating its high uptake; however, the high uptakes of **2** and **3** in liver compared to that of **1** undermined the prominence of tumor accumulation for **2** and **3**. The % ID/g ratios of tumor and liver were 0.32, 0.08, and 0.05 for **1**, **2**, and **3**, respectively, at 24 h postinjection. At 48 and 72 h the tumor contrast became higher for **1** as it was cleared rapidly from spleen and liver (compared to tumor), resulting in an improved tumor image at 48 and 72 h postinjection. In the cases of both **2** and **3**, no significant improvement was observed over time.

The % ID/g ratio of tumor and liver was 0.56, 0.13, and 0.06 for **1**, **2**, and **3**, respectively, at 48 h postinjection.

The tumor volume in each study was obtained by first manually placing an elliptical cylinder that contains the tumor volumes and then counting the voxels with intensity greater than 25% of the maximum of the cylinder volume.

**Comparative Biodistribution of  $^{124}\text{I}$ -Photosensitizer **1** in C3H (RIF Tumors) and BALB/c Mice (Colon-26 Tumors).** On the basis of the results that the lead compound **1** had the best tumor specificity in mice with RIF tumors, we tested it in BALB/c mice bearing Colon-26 tumors by PET imaging and biodistribution studies. Four mice per time point were sacrificed for comparing the biodistribution of **1** in two tumor models. As can be seen in Figure 3, compound **1** ( $^{124}\text{I}$ -labeled) produced higher tumor accumulation in Colon-26 tumor than the RIF tumor at each time point.

The calculated uptake value of compound **1** in Colon-26 tumor was 4.6% ID/g, 4.4% ID/g, 2.5% ID/g, and 2.0% ID/g,

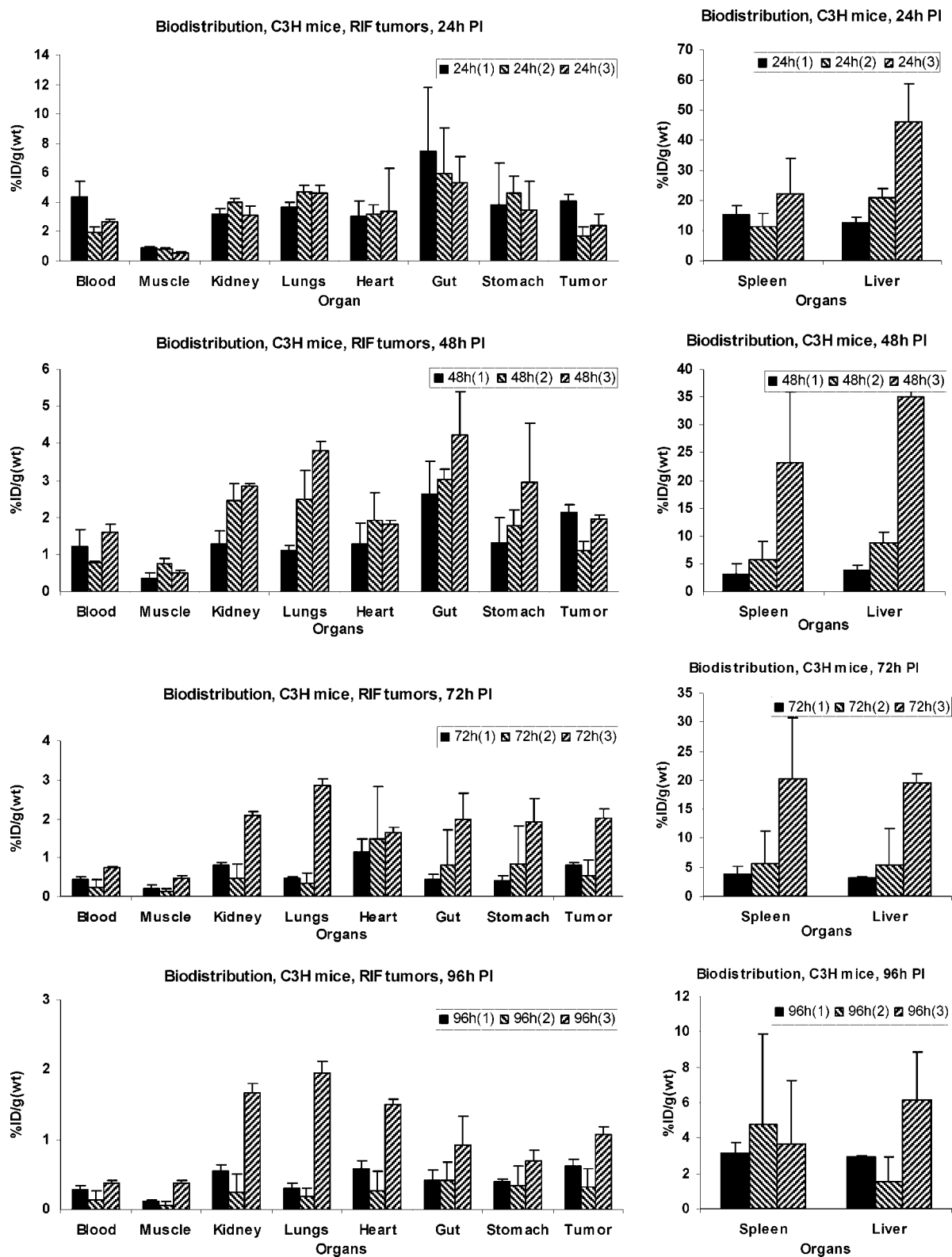


**Figure 2.** Comparative in vivo biodistribution of **1**, **2**, and **3** at selected time points in C3H mice implanted with RIF tumors. Values represent the mean from three or four mice per group.

while in RIF tumor it was 4.1% ID/g, 2.1% ID/g, 0.8% ID/g, and 0.6% ID/g at 24, 48, 72, and 96 h postinjection, respectively. Though compound **1** produced similar uptake at 24 h postinjection in both Colon-26 and RIF tumors, the uptake value in Colon-26 was 2-fold higher at 48 h and 3-fold higher at 72 and 96 h postinjection. These data suggest that the clearance rate of photosensitizer **1** from other organs and in RIF tumors is faster than in Colon-26 tumors. Also, compound **1** showed

slightly higher blood uptake in BALB/c mice than C3H mice. Interestingly, in other organs, compound **1** produced lower uptake in BALB/c mice than the C3H mice. The higher uptake of **1** in Colon-26 tumors compared to RIF tumors and its relatively lower organs' uptake in BALB/c mice may be responsible for enhanced tumor images.

The mice were imaged at 24, 48, 72, and 96 h postinjection of  $^{124}\text{I}$ -labeled **1**, and as can be seen from Figure 4, the PET

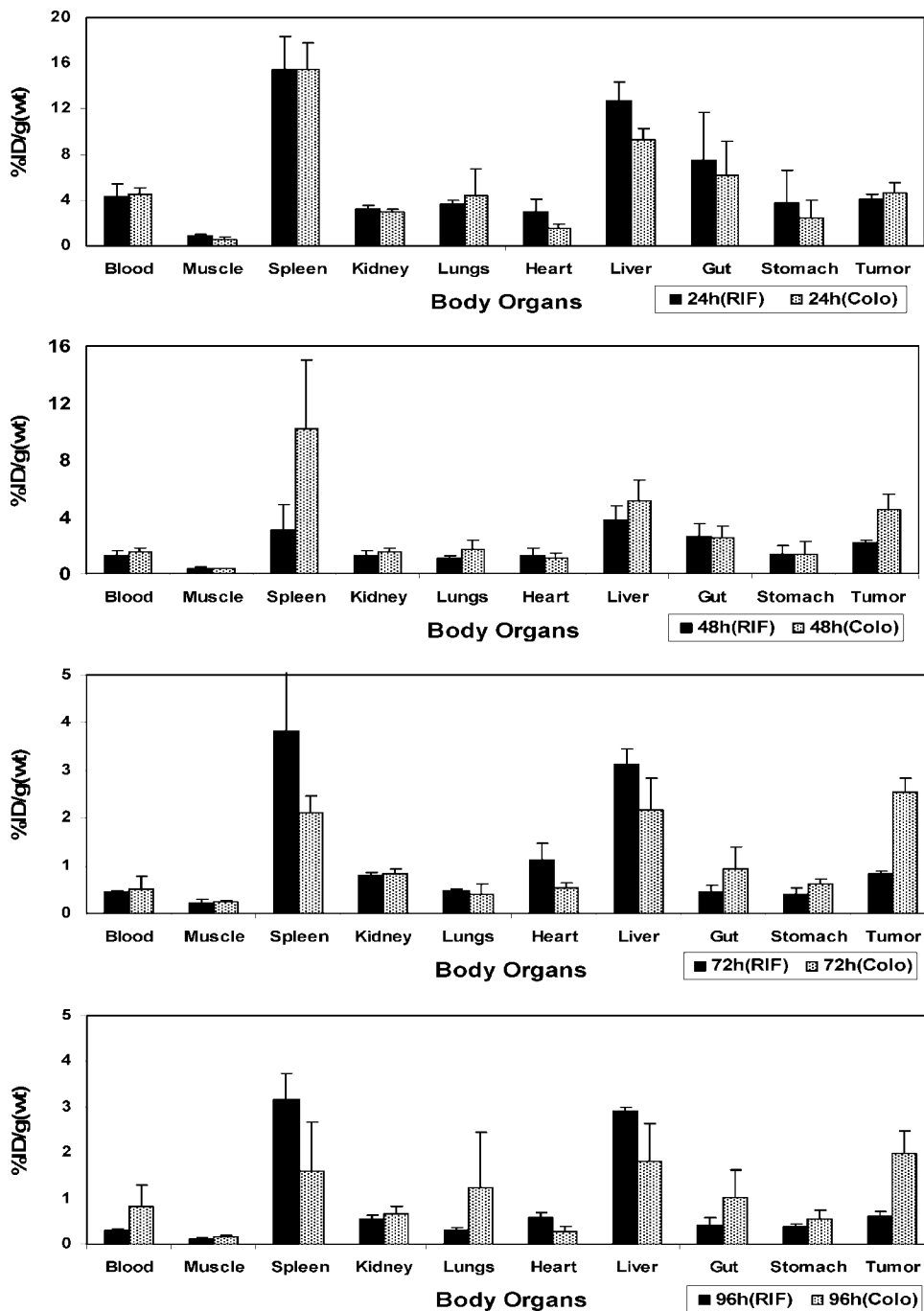


**Figure 3.** Comparative in vivo biodistribution of **1** in C3H mice (RIF tumors) and BALB/c (Colon-26 tumors) at selected time points. Values represent the mean from three or four mice per group.

images of a BALB/c mouse bearing Colon-26 tumor, the tumor was progressively more visible over time as a result of elevated tumor uptake compared to other organs.

To quantify the visibility of tumor in the images, the tumor uptake in each study was measured in terms of a relative uptake value (RUV), which is defined as

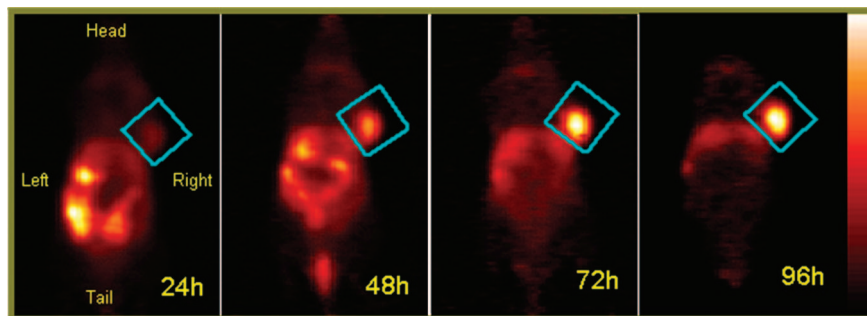
$$RUV = \frac{[\text{max voxel activity in tumor (Bq/cc)}]}{\{[\text{total body activity in image (Bq)}] / [\text{total body volume in image (cc)}]}}$$

The animal's body volume in the image was delineated by defining an isocontour ROI with the ROI's lower threshold set at about 3–6% of the maximum voxel intensity of the data set and manually adjusted according to visual inspection. Using

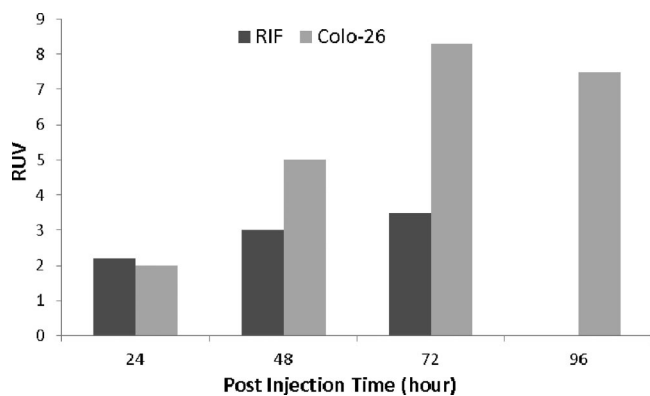
RUV avoids the need to collect the activity excreted through physiological process (excrements) from the time of injection to scan acquisition and reflects the tumor uptake within the interested body section in the same way as the more well-known SUV. The RUV values for images obtained are shown in Figure 5. The RUV value for the <sup>18</sup>F-FDG study was 4.0, slightly higher than that of the <sup>124</sup>I-**1** tracer applied to RIF tumor but lower than the Colon-26 tumor with <sup>124</sup>I-**1** tracer at 48 h postinjection. The Colon-26 tumor showed a higher RUV values than RIF tumor after 48 h of injection of <sup>124</sup>I-**1** agent.

Figure 6 shows the relative activity in tumor compared to the activity in the whole section of body imaged. The relative tumor activity value for the <sup>18</sup>F-FDG RIF tumor study was 0.035, similar to that of <sup>124</sup>I-**1** tracer in RIF tumor, which





**Figure 4.** Coronal view PET images of a BALB/c mice bearing Colon-26 tumors on the right shoulder injected with 150  $\mu\text{Ci}^{124}\text{I}$  of compound **1**. The studies were acquired for 30 min at 24, 48, 72, and 96 h postinjection. The tumor was identified to be within the region defined by a cylinder indicated by the blue rectangle in each image. The color palette (shown on the right) for each image shown was scaled to the min/max of each data set.



**Figure 5.** Comparison of RIF and Colon-26 tumor RUF with  $^{124}\text{I}$ -compound **1**.

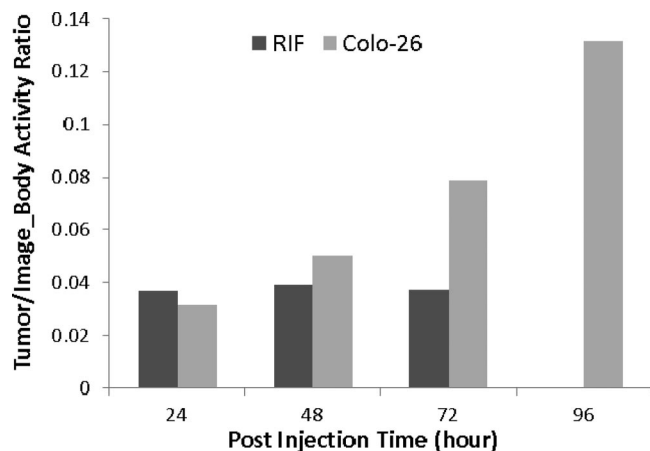


**Figure 6.** Comparison of RIF and Colon-26 tumor activity to whole body activity ratio over time with  $^{124}\text{I}$ -compound **1**. Both activity values were directly derived from images. Note the increasing activity in the Colon-26 tumor.

remained about constant for the three postinjection scans over a 3 day period. The Colon-26 tumor, however, showed increasing relative quantity of activity in the tumor. This explains the increasing prominence of Colon-26 tumor in images over time.

**Comparative in Vitro Uptake and PDT Efficacy.** The cell uptake of photosensitizer **1** and the corresponding galactose and glucose analogues **2** and **3**, respectively, were measured at 3 and 24 h postinjection by fluorescence (see the Experimental Section). As can be seen from Figure 7, all three compounds with or without a carbohydrate moiety showed higher uptake at 24 h postincubation.

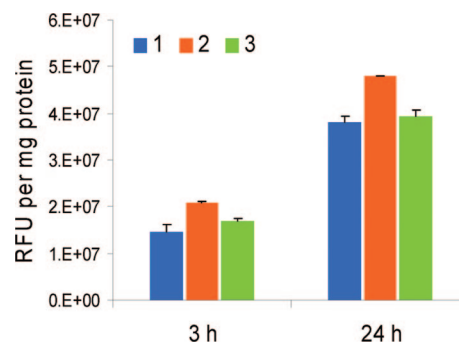


**Figure 7.** In vitro uptake (RIF cells) of **1**, **2**, and **3** at 3 and 24 h after incubation.

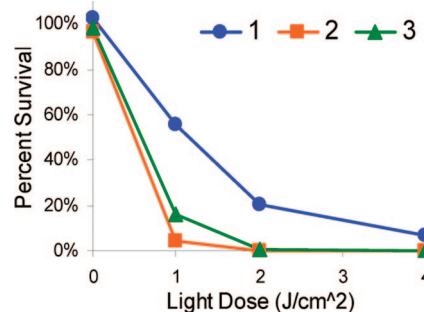


**Figure 8.** In vitro phototoxicity (RIF cells) of **1**, **2**, and **3** (0.25  $\mu\text{M}$ ) at 24 h after incubation.

The photosensitizing abilities of compound **1** and its glucose conjugate **2** and the galactose conjugate **3** were tested in radiation-induced fibrosarcoma (RIF) cells at variable concentrations (0.25, 0.5, 0.25, 1, 2, and 5  $\mu\text{M}$ ), various light doses (0, 1, 2, 4 J/cm<sup>2</sup>) and two incubation time points (4 and 24 h). A drug and light dose-dependent response was observed as determined by the MTT assay. From the results summarized in Figure 8 (only 24 h postincubation results are shown), it can be seen that both the carbohydrate conjugates **2** and **3** are more effective than the corresponding non-carbohydrate analogue **1** at the given conditions.

**In Vivo PDT Efficacy of Pyropheophorbide-*a* 1 and Its Glucose Conjugate 2 and the Galactose Conjugate 3.** For determining the in vivo PDT efficacy of the title compounds, the C3H mice (5 mice/group) bearing RIF tumors (4–5 mm in diameter) were injected intravenously at variable drug doses (0.5, 1.0, and 1.5  $\mu\text{mol/kg}$ ). The tumor area was then irradiated with a 1 cm<sup>2</sup> laser light (665 nm, 135 J/cm<sup>2</sup>, 75 mW/cm<sup>2</sup> for 30 min) at 24 h postinjection. The tumor regrowth was observed daily, and when the tumor size reached the threshold of 400

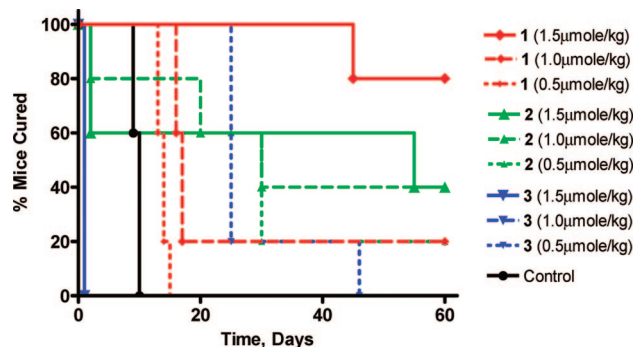


**Figure 9.** Kaplan–Meier plot for compounds **1**, **2**, and **3** at various drug doses in C3H mice bearing RIF tumor on shoulder (5 mice/group): light dose, 135 J/cm<sup>2</sup>, 75 mW/cm<sup>2</sup> for 30 min at 24 h postinjection.

mm<sup>3</sup>, the mice were sacrificed. From the results summarized in Figure 9, it can be seen that at the lowest drug dose (0.50 μmol/kg), one out of five mice was tumor-free with the glucose conjugate **2**, whereas the nonconjugate **1** and galactose conjugate **3** did not show any tumor response, though between **1** and **3**, **3** showed improved tumor cure. Upon an increased drug dose (1.00 μmol/kg), two out of five mice were tumor-free for **2** while one out of five mice was tumor free for compound **1**. For compound **3**, this dose was found to be toxic and all five mice died within 24 h after PDT. When the dose was escalated to 1.5 μmol/kg, the cure rate for compound **1** showed a significant increase in photosensitizing ability and four out of five mice were tumor-free at day 60. At the same drug dose and light treatment parameters some toxicity was observed for compound **2**, where two mice died within 24 h after PDT and two out of remaining three mice were tumor free by day 60. This drug dose was found to be too toxic for compound **3** and all five mice died within 24 h after light treatment. Further evaluation of these photosensitizers at variable drug and light doses in different tumor models is currently in progress.

## Conclusion

PDT is a localized form of cancer treatment and has several advantages over other cancer treatment modalities. Most of the porphyrin-based compounds and those evaluated in our present study show optimal tumor uptake at >24 h. Therefore, for development of a single bifunctional agent for PET imaging and PDT, it is necessary to label the desired photosensitizer(s) with radionuclide having a long half-life. With <sup>124</sup>I- labeled (half-life of 4.2 days) agent **1**, we were able to detect the tumors by PET imaging in two different models (RIF and Colon-26). The long residence time of the photosensitizer in tumor, as confirmed by the RUV and relative tumor activity values, also indicated great therapeutic potential. Compared to compound **1**, the corresponding glucose **2** and galactose **3** analogues showed higher uptake in both Colon-26 and RIF cells. However, the in vivo biodistribution results obtained from the C3H mice bearing RIF tumors revealed that between the glucose and galactose conjugates, the galactose conjugate **3** had higher tumor uptake. Interestingly, because of a high uptake of the carbohydrate derivatives in liver and spleen, the parent molecule **1** produced the best tumor contrast in both RIF and Colon-26 tumor models. Further studies to investigate the imaging potential of these and a series of PEG analogues with variable lipophilicity over <sup>18</sup>F-FDG in a series of tumor models are currently in progress.

## Experimental Section

**Chemistry.** All chemicals were of reagent grade and used as such. Solvents were dried using standard methods. Reactions were

carried out under nitrogen/argon atmosphere and were monitored by precoated (0.20 mm) silica TLC plastic sheet (20 cm × 20 cm) strips (POLYGRAM SIL N-HR) and/or UV–visible spectroscopy. Silica gel 60 (70–230 mesh, Merck) was used for column chromatography. Melting points were determined on a Fisher-Johns melting point apparatus. UV–visible spectra were recorded on a Varian (Cary 50 Bio) spectrophotometer. <sup>1</sup>H NMR spectra were recorded on a Bruker AMX 400 MHz NMR spectrometer at 303 K. Proton chemical shifts (δ) are reported in parts per million (ppm) relative to CDCl<sub>3</sub> (7.26 ppm), pyridine-*d*<sub>5</sub> (7.22 ppm, most downfield), or TMS (0.00 ppm). Coupling constants (*J*) are reported in hertz (Hz), and s, d, t, q, p, m, and br refer to singlet, doublet, triplet, quartet, pentet, multiplet, and broad, respectively. HRMS data were obtained from the mass spectroscopy facility of Michigan State University. Analytical HPLC was used to assess the purity of compounds. A Waters (Milford, MA) system including Waters 600 controller, Delta 600 pump, and 996 photodiode array detector was used. Reverse phase Symmetry C18, 5 μm, 4.6 × 150 mm column (Waters) was used under isocratic setting of MeOH/H<sub>2</sub>O for final compounds (**1–3** and their trimethyltin analogues). Solvent flow rate was kept constant at 1.00 mL/min, and the detector was set at 254, 410, 535, and 660 nm. All final products were found to be >95% pure, and their retention time is reported in the characterization section. Cold reactions were first carried out, and the products were analyzed in the above HPLC system. However, in the case of final I-124 radiolabeling (hot reaction), HPLC data obtained from the above system were transferred to another system comprising a Chrom Tech Iso-2000 pump, Hitachi L-4000 UV detector, and a radiation detector. These detectors are connected to a computer with HP Chemstation software via HP 35900E interface. A Bioscan system 200 imaging scanner was used for thin layer chromatography of the radiolabeled compounds.

**Synthesis of 3-{1'-(*m*-Iodobenzyloxy)ethyl}pyropheophorbide-*a* Methyl Ester (**1**).** It was prepared by following the reported procedure.<sup>12</sup> Yield: 77%. Analytical RP HPLC (95/5 MeOH/H<sub>2</sub>O, Symmetry): *t*<sub>R</sub> = 20.97 min, >96%. UV–visible (CH<sub>2</sub>Cl<sub>2</sub>): 662 (4.75 × 10<sup>4</sup>), 536 (1.08 × 10<sup>4</sup>), 505 (1.18 × 10<sup>4</sup>), 410 (1.45 × 10<sup>5</sup>). <sup>1</sup>H NMR (CDCl<sub>3</sub>, 400 MHz): δ 9.76, 9.55, and 8.56 (all s, 1H, meso-H), 7.76 (s, 1H, ArH), 7.64 (d, *J* = 6.8, 1H, ArH), 7.30 (d, *J* = 8.0, 1H, ArH), 7.05 (t, *J* = 8.2, 1H, ArH), 6.00 (q, *J* = 6.9, 1H, 3<sup>1</sup>-H), 5.28 (d, *J* = 19.8, 1H, 13<sup>2</sup>-CH<sub>2</sub>), 5.13 (d, *J* = 19.8, 1H, 13<sup>2</sup>-CH<sub>2</sub>), 4.70 (d, *J* = 12.0, 1H, OCH<sub>2</sub>Ar), 4.56 (dd, *J* = 3.2, 11.6, 1H, OCH<sub>2</sub>Ar), 4.48–4.53 (m, 1H, 18-H), 4.30–4.33 (m, 1H, 17-H), 3.72 (q, *J* = 8.0, 2H, 8-CH<sub>2</sub>CH<sub>3</sub>), 3.69, 3.61, 3.38 and 3.21 (all s, all 3H, for 17<sup>2</sup>-CO<sub>2</sub>CH<sub>3</sub> and 3 × ring CH<sub>3</sub>), 2.66–2.74, 2.52–2.61 and 2.23–2.37 (m, 4H, 17<sup>1</sup> and 17<sup>2</sup>-H), 2.18 (dd, *J* = 2.8, 6.4, 3H, 3<sup>1</sup>-CH<sub>3</sub>), 1.83 (d, *J* = 8.0, 3H, 18-CH<sub>3</sub>), 1.72 (t, *J* = 7.6, 3H, 8-CH<sub>2</sub>CH<sub>3</sub>), 0.41 (brs, 1H, NH), –1.71 (brs, 1H, NH). HRMS for C<sub>41</sub>H<sub>43</sub>N<sub>4</sub>O<sub>4</sub>I: 782.2329 (calculated); 783.24 (found, MH<sup>+</sup>). Anal. Calcd for C<sub>41</sub>H<sub>43</sub>N<sub>4</sub>O<sub>4</sub>I: C, 62.91; H, 5.54; N, 7.16; I, 16.21. Found: C, 62.60; H, 5.59; N, 7.13; I, 16.45.

**Synthesis of 3-{1'-(*m*-Trimethylstannylbenzyloxy)ethyl}pyropheophorbide-*a* Methyl Ester (**12**).** It was synthesized following the reported procedure.<sup>12</sup> Yield: 80%. Analytical RP HPLC (95/5 MeOH/H<sub>2</sub>O): *t*<sub>R</sub> = 27.88min, >96%. UV–visible (CH<sub>2</sub>Cl<sub>2</sub>): 662 (4.75 × 10<sup>4</sup>), 605 (6.94 × 10<sup>3</sup>), 537 (7.77 × 10<sup>3</sup>), 506 (7.66 × 10<sup>3</sup>), 410 (9.58 × 10<sup>4</sup>). <sup>1</sup>H NMR (CDCl<sub>3</sub>, 400 MHz): δ 9.76, 9.54, and 8.55 (all s, 1H, meso-H), 7.43 (m, 2H, ArH), 7.36 (m, 2H, ArH), 6.01 (q, *J* = 6.7, 1H, 3<sup>1</sup>-H), 5.27 (d, *J* = 19.1, 1H, 13<sup>2</sup>-CH<sub>2</sub>), 5.12 (d, *J* = 19.1, 1H, 13<sup>2</sup>-CH<sub>2</sub>), 4.78 (dd, *J* = 5.4, 11.9, 1H, OCH<sub>2</sub>Ar), 4.61 (dd, *J* = 1.7, 12.0, 1H, OCH<sub>2</sub>Ar), 4.50 (q, *J* = 7.4, 1H, 18-H), 4.32 (d, *J* = 8.8, 1H, 17-H), 3.72 (q, *J* = 7.8, 2H, 8-CH<sub>2</sub>CH<sub>3</sub>), 3.69, 3.61, 3.37, and 3.18 (all s, all 3H, for 17<sup>2</sup>-CO<sub>2</sub>CH<sub>3</sub> and 3 × ring CH<sub>3</sub>), 2.66–2.75, 2.52–2.61, and 2.23–2.37 (m, 4H, 17<sup>1</sup> and 17<sup>2</sup>-H), 2.16 (m, 3H, 3<sup>1</sup>-CH<sub>3</sub>), 1.83 (d, *J* = 7.2, 3H, 18-CH<sub>3</sub>), 1.72 (t, *J* = 7.6, 3H, 8-CH<sub>2</sub>CH<sub>3</sub>), 0.45 (brs, 1H, NH), 0.19 (s, 9H, Sn(CH<sub>3</sub>)<sub>3</sub>), –0.59 (brs, 1H, NH). Mass: calculated for C<sub>45</sub>H<sub>52</sub>N<sub>4</sub>O<sub>4</sub>Sn, 831; found, 854 (M<sup>+</sup> + Na). Anal. Calcd for C<sub>45</sub>H<sub>52</sub>N<sub>4</sub>O<sub>4</sub>Sn: C, 64.99; H, 6.30; N, 6.74. Found: C, 64.56; H, 6.66; N, 6.59.

**Synthesis of 3-{1'-(*m*-Iodobenzyloxy)ethyl}pyropheophorbide-*a* (4).** Aqueous LiOH (400 mg in 12 mL of H<sub>2</sub>O, purged with argon) was added to a solution of 3-{1'-(3-iodobenzyloxy)ethyl}pyropheophorbide-*a* methyl ester (**1**) (200 mg, 0.25 mmol) in dry THF/MeOH (25:8 mL), and the reaction mixture was stirred under argon at room temperature for 2 h. The reaction mixture was neutralized with 2% AcOH in H<sub>2</sub>O, and compound was extracted with CH<sub>2</sub>Cl<sub>2</sub> (100 mL). The organic layer was washed with H<sub>2</sub>O (2 × 100 mL), dried over Na<sub>2</sub>SO<sub>4</sub>, concentrated, and precipitated with hexanes to yield 185 mg (95%) crude product **6**, which was found to be pure enough for further use. UV-visible (MeOH/CH<sub>2</sub>Cl<sub>2</sub>): 663 (4.75 × 10<sup>4</sup>), 605 (6.81 × 10<sup>3</sup>), 539 (6.81 × 10<sup>3</sup>), 506 (6.61 × 10<sup>3</sup>), 411 (9.52 × 10<sup>4</sup>). <sup>1</sup>H NMR (CDCl<sub>3</sub>, 400 MHz): δ 9.72, 9.44, and 8.53 (all s, 1H, meso-H), 7.74 (s, 1H, ArH), 7.61 (d, *J* = 8.0, 1H, ArH), 7.28 (m, 1H, ArH), 7.03 (m, 1H, ArH), 5.95 (q, *J* = 6.8, 1H, 3<sup>1</sup>-H), 5.25 (d, *J* = 20.0, 1H, 13<sup>2</sup>-CH<sub>2</sub>), 5.10 (d, *J* = 20.0, 1H, 13<sup>2</sup>-CH<sub>2</sub>), 4.65 (dd, *J* = 4.0, 12.0, 1H, OCH<sub>2</sub>Ar), 4.50 (m, 2H, OCH<sub>2</sub>Ar and 18-H), 4.28 (d, *J* = 7.6, 1H, 17-H), 3.67 (q, *J* = 7.6, 2H, 8-CH<sub>2</sub>CH<sub>3</sub>), 3.58, 3.34, and 3.18 (all s, all 3H, for 3 × ring CH<sub>3</sub>), 2.55–2.72 and 2.20–2.35 (m, 4H, 17<sup>1</sup> and 17<sup>2</sup>-H), 2.15 (m, 3H, 3<sup>1</sup>-CH<sub>3</sub>), 1.78 (d, *J* = 7.6, 3H, 18-CH<sub>3</sub>), 1.68 (t, *J* = 7.2, 3H, 8-CH<sub>2</sub>CH<sub>3</sub>), 0.02 (brs, 1H, NH), –1.70 (brs, 1H, NH). HRMS for C<sub>40</sub>H<sub>41</sub>N<sub>4</sub>O<sub>4</sub>I: 768.2174 (calculated); 769.2207 (found, MH<sup>+</sup>).

**Synthesis of 3-{1'-(*m*-Iodobenzyloxy)ethyl}pyropheophorbide-*a* Succinimidyl Ester (**5**).** Compound **4** (100 mg, 0.13 mmol) was activated with DCC (40 mg, 0.20 mmol) and *N*-hydroxysuccinimide (25 mg, 0.22 mmol) in DMF (3 mL). After the mixture was stirred at room temperature overnight, DCU was filtered off and the filtrate was concentrated and chromatographed over a silica column with 2.5% MeOH in CH<sub>2</sub>Cl<sub>2</sub> as eluant. The product obtained was precipitated with CH<sub>2</sub>Cl<sub>2</sub>–hexanes, filtered, and washed with chilled CH<sub>2</sub>Cl<sub>2</sub> (2 × 2 mL) to remove any traces of residual DCU to yield 85 mg (75%) of pure product. UV-visible (CH<sub>2</sub>Cl<sub>2</sub>): 662 (4.75 × 10<sup>4</sup>), 605 (8.55 × 10<sup>3</sup>), 538 (9.21 × 10<sup>3</sup>), 506 (8.86 × 10<sup>3</sup>), 410 (9.20 × 10<sup>4</sup>). <sup>1</sup>H NMR (CDCl<sub>3</sub>, 400 MHz): δ 9.72, 9.44, and 8.53 (all s, 1H, meso-H), 7.74 (s, 1H, ArH), 7.61 (m, 1H, ArH), 7.28 (m, 1H, ArH), 7.03 (m, 1H, ArH), 5.95 (q, *J* = 6.8, 1H, 3<sup>1</sup>-H), 5.25 (d, *J* = 20.0, 1H, 13<sup>2</sup>-CH<sub>2</sub>), 5.10 (d, *J* = 20.0, 1H, 13<sup>2</sup>-CH<sub>2</sub>), 4.65 (dd, *J* = 4.0, 12.0, 1H, OCH<sub>2</sub>Ar), 4.50 (m, 2H, OCH<sub>2</sub>Ar and 18-H), 4.28 (d, *J* = 7.6, 1H, 17-H), 3.67 (q, *J* = 7.6, 2H, 8-CH<sub>2</sub>CH<sub>3</sub>), 3.58, 3.34, and 3.18 (all s, all 3H, for 3 × ring CH<sub>3</sub>), 2.55–2.72 (m, 6H, succinimidyl CO(CH<sub>2</sub>)<sub>2</sub>CO and 17<sup>1</sup>-H), 2.20–2.35 (m, 2H, 17<sup>2</sup>-H), 2.15 (m, 3H, 3<sup>1</sup>-CH<sub>3</sub>), 1.80 (d, *J* = 7.6, 3H, 18-CH<sub>3</sub>), 1.68 (t, *J* = 7.2, 3H, 8-CH<sub>2</sub>CH<sub>3</sub>), 0.02 (brs, 1H, NH), –1.70 (brs, 1H, NH). HRMS for C<sub>44</sub>H<sub>44</sub>N<sub>5</sub>O<sub>6</sub>I: 865.2338 (calculated); 866.2312 (found, MH<sup>+</sup>).

**Synthesis of 3-{1'-(*m*-Iodobenzyloxy)ethyl}-17<sup>2</sup>-(2-amino-2-deoxy)glucosamidepyropheophorbide-*a* (**2**).** To a solution of sodium methoxide (150 μL of 25% by wt) and anhydrous DMSO (2.5 mL) under argon was added *D*-glucosamine hydrochloride (150 mg), and reaction mixture was stirred at room temperature for 1.5 h (clear solution becomes turbid and pale in color). Then 0.8 mL of this reaction mixture was added to 3-{1'-(3-iodobenzyloxy)ethyl}pyropheophorbide-*a* succinimidyl ester **5** (50 mg, 0.06 mmol) and the resultant reaction mixture was stirred at room temperature overnight. Water (10 mL) was poured into the reaction mixture and the solid that separated out was filtered and chromatographed over silica column using 10% MeOH in CH<sub>2</sub>Cl<sub>2</sub> as eluant to afford 40 mg (75%) of **2**. Analytical RP HPLC (95/5 MeOH/H<sub>2</sub>O, Symmetry): *t*<sub>R</sub> = 8.17 min, >96%. UV-visible (CH<sub>2</sub>Cl<sub>2</sub>): 663 (4.75 × 10<sup>4</sup>), 606 (7.08 × 10<sup>3</sup>), 535 (8.69 × 10<sup>3</sup>), 506 (8.84 × 10<sup>3</sup>), 410 (8.89 × 10<sup>4</sup>). <sup>1</sup>H NMR (pyridine-*d*<sub>5</sub>, 400 MHz): δ 10.20 (splits, 1H, meso-H), 9.96 (s, 1H, meso-H), 8.82 (s, 1H, meso-H), 8.58 (brs, 1H, CONH), 8.10 (s, 1H, ArH), 7.77 (d, *J* = 7.6, 1H, ArH), 7.53 (d, *J* = 8.0, 1H, ArH), 7.15 (t, *J* = 7.8, 1H, ArH), 6.24 (t, *J* = 6.6, 1H, Glu-H), 5.95 (s, 1H, 3<sup>1</sup>-H), 5.42 (d, *J* = 20.4, 1H, 13<sup>2</sup>-CH<sub>2</sub>), 5.18 (d, *J* = 19.6, 1H, 13<sup>2</sup>-CH<sub>2</sub>), 4.90 (brs, 6H, OCH<sub>2</sub>Ar and Glu-OH), 4.48–4.85 (m, 6H, Glu-H), 4.36 (dd, *J* = 5.8, 11.8, 1H, H-18), 4.26 (t, *J* = 9.0, 1H, H-17), 3.79 (q, *J* = 7.47, 2H, 8-CH<sub>2</sub>CH<sub>3</sub>), 3.73 (s, 3H, ring CH<sub>3</sub>), 3.41 (s, 3H, ring CH<sub>3</sub>), 3.29

(s, 3H, ring CH<sub>3</sub>), 3.00–3.10 (m, 1H, 17<sup>1</sup>-H), 2.80–2.90 (m, 1H, 17<sup>2</sup>-H), 2.65–2.75 (m, 1H, 17<sup>1</sup>-H), 2.50–2.60 (m, 1H, 17<sup>2</sup>-H), 2.28 (d, *J* = 6.4, 3H, 3<sup>1</sup>-CH<sub>3</sub>), 1.87 (d, *J* = 6.4, 3H, 18-CH<sub>3</sub>), 1.73 (t, *J* = 7.6, 3H, 8-CH<sub>2</sub>CH<sub>3</sub>), 0.70 (brs, 1H, NH), –1.70 (brs, 1H, NH). HRMS for C<sub>46</sub>H<sub>52</sub>N<sub>5</sub>O<sub>8</sub>I: 929.2862 (calculated); 930.2854 (found, MH<sup>+</sup>).

**Synthesis of 3-{1'-(*m*-Trimethylstannylbenzyloxy)ethyl}pyropheophorbide-*a* (**7**).** To a solution of **4** (70 mg, 0.09 mmol) in dry THF (20 mL) were added hexamethylditin (0.1 mL, 0.48 mmol) and bis(triphenylphosphine)palladium(II) dichloride (20 mg), and the reaction mixture was stirred at room temperature overnight. After removal of the solvent under vacuum to dryness, the crude mixture was purified over silica gel column using 1% MeOH in CH<sub>2</sub>Cl<sub>2</sub> as eluant to yield 40 mg (55%) of compound **7**. UV-visible (CH<sub>2</sub>Cl<sub>2</sub>): 662 (4.75 × 10<sup>4</sup>), 606 (8.46 × 10<sup>3</sup>), 538 (9.16 × 10<sup>3</sup>), 507 (9.20 × 10<sup>3</sup>), 411 (9.57 × 10<sup>4</sup>). <sup>1</sup>H NMR (CDCl<sub>3</sub>, 400 MHz): δ 9.73, 9.40, and 8.52 (all s, 1H, meso-H), 7.42 (m, 2H, ArH), 7.34 (m, 2H, ArH), 5.98 (m, 1H, 3<sup>1</sup>-H), 5.27 (d, *J* = 19.6, 1H, 13<sup>2</sup>-CH<sub>2</sub>), 5.10 (d, *J* = 19.6, 1H, 13<sup>2</sup>-CH<sub>2</sub>), 4.75 (dd, *J* = 3.0, 11.2, 1H, OCH<sub>2</sub>Ar), 4.58 (dd, *J* = 1.8, 12.0, 1H, OCH<sub>2</sub>Ar), 4.48 (q, *J* = 7.2, 1H, 18-H), 4.29 (d, *J* = 8.0, 1H, 17-H), 3.64 (q, *J* = 7.8, 2H, 8-CH<sub>2</sub>CH<sub>3</sub>), 3.55 (s, 3H, ring CH<sub>3</sub>), 3.34 (s, 3H, ring CH<sub>3</sub>), 3.15 (s, 3H, ring CH<sub>3</sub>), 2.60–2.75 and 2.25–2.40 (m, 4H, 17<sup>1</sup> and 17<sup>2</sup>-H), 2.13 (m, 3H, 3<sup>1</sup>-CH<sub>3</sub>), 1.78 (d, *J* = 7.2, 3H, 18-CH<sub>3</sub>), 1.66 (t, *J* = 7.2, 3H, 8-CH<sub>2</sub>CH<sub>3</sub>), 0.17 (s, 9H, Sn(CH<sub>3</sub>)<sub>3</sub>), 0.05 (brs, 1H, NH), –1.65 (brs, 1H, NH). HRMS for C<sub>43</sub>H<sub>50</sub>N<sub>4</sub>O<sub>4</sub>Sn: 806.2853 (calculated); 807.2848 (found, MH<sup>+</sup>).

**Synthesis of 3-{1'-(*m*-Trimethylstannylbenzyloxy)ethyl}pyropheophorbide-*a* Succinimidyl Ester (**8**).** Compound **7** (45 mg, 0.06 mmol) was activated with DCC (20 mg, 0.10 mmol) and *N*-hydroxysuccinimide (15 mg, 0.13 mmol) in DMF (2 mL). After the mixture was stirred overnight at room temperature, DCU was filtered off and the filtrate was concentrated and chromatographed over silica column with 2.5% MeOH in CH<sub>2</sub>Cl<sub>2</sub> as eluant. The product obtained was precipitated with CH<sub>2</sub>Cl<sub>2</sub>–hexanes, filtered, and washed with chilled CH<sub>2</sub>Cl<sub>2</sub> (2 × 2 mL) to remove any traces of residual DCU to yield 45 mg (90%) of pure product. UV-visible (CH<sub>2</sub>Cl<sub>2</sub>): 662 (4.75 × 10<sup>4</sup>), 606 (7.84 × 10<sup>3</sup>), 538 (8.28 × 10<sup>3</sup>), 506 (8.88 × 10<sup>3</sup>), 411 (9.37 × 10<sup>4</sup>). <sup>1</sup>H NMR (CDCl<sub>3</sub>, 400 MHz): δ 9.77 (splits, 1H, meso-H), 9.53 and 8.56 (both s, 1H, meso-H), 7.42 (m, 2H, ArH), 7.36 (m, 2H, ArH), 6.00 (q, *J* = 6.7, 1H, 3<sup>1</sup>-H), 5.23 (d, *J* = 20.4, 1H, 13<sup>2</sup>-CH<sub>2</sub>), 5.15 (d, *J* = 19.6, 1H, 13<sup>2</sup>-CH<sub>2</sub>), 4.77 (dd, *J* = 5.2, 11.6, 1H, OCH<sub>2</sub>Ar), 4.60 (dd, *J* = 1.8, 11.8, 1H, OCH<sub>2</sub>Ar), 4.49–4.55 (m, 1H, 18-H), 4.43 (d, *J* = 9.2, 1H, 17-H), 3.72 (q, *J* = 8.0, 2H, 8-CH<sub>2</sub>CH<sub>3</sub>), 3.68, 3.37, and 3.17 (all s, all 3H, for 3 × ring CH<sub>3</sub>), 2.87 (brs, 6H, succinimidyl CO(CH<sub>2</sub>)<sub>2</sub>CO and 17<sup>1</sup>-H), 2.56–2.63 and 2.25–2.35 (m, 2H, 17<sup>2</sup>-H), 2.15 (dd, *J* = 3.6, 6.4, 3H, 3<sup>2</sup>-CH<sub>3</sub>), 1.82 (d, *J* = 7.2, 3H, 18-CH<sub>3</sub>), 1.70 (t, *J* = 7.2, 3H, 8-CH<sub>2</sub>CH<sub>3</sub>), 0.44 (brs, 1H, NH), 0.18 (s, 9H, Sn(CH<sub>3</sub>)<sub>3</sub>), –1.70 (brs, 1H, NH). HRMS for C<sub>47</sub>H<sub>53</sub>N<sub>5</sub>O<sub>6</sub>Sn: 903.3017 (calculated); 904.3009 (found, MH<sup>+</sup>).

**Synthesis of 3-{1'-(*m*-Trimethylstannylbenzyloxy)ethyl}-17<sup>2</sup>-(2-amino-2-deoxy)glucosamidepyropheophorbide-*a* (**9**).** It was synthesized using the respective starting material **10** by following the procedure reported for **2**. Yield: 75%. Analytical RP HPLC (95/5 MeOH/H<sub>2</sub>O, Symmetry): *t*<sub>R</sub> = 10.51 min, >96%. UV-visible (MeOH/CH<sub>2</sub>Cl<sub>2</sub>): 662 (4.75 × 10<sup>4</sup>), 605 (8.62 × 10<sup>3</sup>), 539 (9.24 × 10<sup>3</sup>), 507 (8.93 × 10<sup>3</sup>), 410 (9.07 × 10<sup>4</sup>). <sup>1</sup>H NMR (pyridine-*d*<sub>5</sub>, 400 MHz): δ 10.24 (splits, 1H, meso-H), 9.95 (s, 1H, meso-H), 8.82 (s, 1H, meso-H), 8.58 (brs, 1H, amidic NH), 7.78 (s, 1H, ArH), 7.67 (m, 1H, ArH), 7.60 (m, 1H, ArH), 7.51 (m, 1H, ArH), 6.28 (m, 1H, 3<sup>1</sup>-H), 5.35–5.45 (m, 2H, 13<sup>2</sup>-CH<sub>2</sub>, Glu-H), 5.18 (d, *J* = 20.0, 1H, 13<sup>2</sup>-CH<sub>2</sub>), 4.80–5.1 (brs, 7H, OCH<sub>2</sub>Ar, Glu-H, Glu-OH), 4.69 (m, 1H, Glu-H), 4.62 (m, 2H, Glu-H), 4.50 (m, 2H, Glu-H), 4.36 (m, 1H, 18-H), 4.26 (m, 1H, 17-H), 3.79 (q, *J* = 7.5, 2H, 8-CH<sub>2</sub>CH<sub>3</sub>), 3.73 (s, 3H, ring CH<sub>3</sub>), 3.44 (d, *J* = 6.4, 3H, ring CH<sub>3</sub>), 3.25 (s, 3H, ring CH<sub>3</sub>), 3.00–3.10 (m, 1H, 17<sup>1</sup>-H), 2.80–2.90 (m, 1H, 17<sup>2</sup>-H), 2.65–2.75 (m, 1H, 17<sup>1</sup>-H), 2.50–2.60 (m, 1H, 17<sup>2</sup>-H), 2.30 (d, *J* = 6.4, 3H, 3<sup>1</sup>-CH<sub>3</sub>), 1.87 (d, *J* = 6.4, 3H, 18-CH<sub>3</sub>), 1.74 (t, *J* = 7.6, 3H, 8-CH<sub>2</sub>CH<sub>3</sub>), 0.73 (brs, 1H, NH), 0.23 (s, 9H,



Sn(CH<sub>3</sub>)<sub>3</sub>), -1.70 (brs, 1H, NH). HRMS for C<sub>49</sub>H<sub>61</sub>N<sub>5</sub>O<sub>8</sub>Sn: 967.3541 (calculated): 968.3534 (found, MH<sup>+</sup>).

**Synthesis of 3-[1'-(*m*-Iodobenzyloxy)ethyl]-17<sup>2</sup>-(1-amino-1-deoxy)-tetraacetogalactosamidepyropheophorbide-a (6).** Compound **4** (30 mg, 0.04 mmol), tetraacetogalactosamine (30 mg, 0.08 mmol) and PyBOP (26 mg, 0.05 mmol) were added to anhydrous DMF (3 mL) under nitrogen, and the reaction mixture was stirred at room temperature overnight. DMF was removed under vacuum, and the crude obtained was purified over silica preparative TLC plate using 5% MeOH in CH<sub>2</sub>Cl<sub>2</sub> as eluant. Yield: 25 mg (60%). <sup>1</sup>H NMR (CDCl<sub>3</sub>, 400 MHz): δ 9.78 (s, 1H, meso-H), 9.54 (s, 1H, meso-H), 8.56 (s, 1H, meso-H), 7.75 (s, 1H, ArH), 7.65 (d, *J* = 7.2, 1H, ArH), 7.32 (d, *J* = 7.6, 1H, ArH), 7.07 (dt, *J* = 0.8, 7.8, 1H, ArH), 6.06 (dd, *J* = 4.0, 9.2, 1H, CONH), 6.01 (q, *J* = 6.8, 1H, 3<sup>1</sup>-H), 5.40 (d, *J* = 3.2, 1H, Gal-H), 5.29 (d, *J* = 19.2, 1H, 13<sup>2</sup>-CH<sub>2</sub>), 5.05–5.25 (m, 3H, 13<sup>2</sup>-H and Gal-H), 4.95 (dt, *J* = 2.4, 10.2, 1H, Gal-H), 4.72 (dd, *J* = 3.2, 12.0, 1H, Gal-H), 4.58 (dd, *J* = 1.8, 11.8, 1H, Gal-H), 4.50 (dq, *J* = 1.2, 6.8, 1H, 18-H), 4.38 (m, 1H, 17-H), 4.05 (m, 2H, OCH<sub>2</sub>Ar), 3.99 (m, 1H, Gal-H), 3.72 (q, *J* = 7.6, 2H, 8-CH<sub>2</sub>CH<sub>3</sub>), 3.67 (s, 3H, ring CH<sub>3</sub>), 3.40 (splits, 3H, ring CH<sub>3</sub>), 3.23 (splits, 3H, ring CH<sub>3</sub>), 2.65–2.75 (m, 1H, 17<sup>1</sup>-H), 2.30–2.45 (m, 2H, 17<sup>2</sup>-H and 17<sup>1</sup>-H), 2.19 (dd, *J* = 3.0, 6.8, 3H, 3<sup>1</sup>-CH<sub>3</sub>), 2.06 (brs, 4H, 17<sup>2</sup>-H and COCH<sub>3</sub>), 2.00 (s, 3H, COCH<sub>3</sub>), 1.96 (s, 3H, COCH<sub>3</sub>), 1.92 (s, 3H, COCH<sub>3</sub>), 1.83 (d, *J* = 7.6, 3H, 18-CH<sub>3</sub>), 1.72 (t, *J* = 7.6, 3H, 8-CH<sub>2</sub>CH<sub>3</sub>), 0.45 (brs, 1H, NH), -1.70 (brs, 1H, NH). HRMS for C<sub>54</sub>H<sub>60</sub>N<sub>5</sub>O<sub>12</sub>I: 1097.3284 (calculated); 1098.3277 (found, MH<sup>+</sup>).

**Synthesis of {1'-(*m*-Iodobenzyloxy)ethyl}-17<sup>2</sup>-(1-amino-1-deoxy)-galactosamidepyropheophorbide-a (3).** To a solution of 1'-(3-iodobenzyloxy)ethyl}-17<sup>2</sup>-(1-amino-1-deoxy)tetraacetogalactosamidepyropheophorbide-a (**6**) (22 mg, 0.02 mmol) in dry CH<sub>2</sub>Cl<sub>2</sub> (5 mL) and dry MeOH (0.5 mL) under nitrogen, sodium methoxide (100 μL) was added, and the reaction mixture was stirred for 20 min at room temperature. The reaction mixture was neutralized with resin and filtered. The filtrate was removed under vacuum and purified by passing through a short silica column using 10% MeOH in CH<sub>2</sub>Cl<sub>2</sub> as eluant to yield 15 mg (80%) of **3**. Analytical RP HPLC (95/5 MeOH/H<sub>2</sub>O, Symmetry): *t*<sub>R</sub> = 8.02 min, >96%. UV-visible (CH<sub>2</sub>Cl<sub>2</sub>): 662 (4.75 × 10<sup>4</sup>), 606 (8.75 × 10<sup>3</sup>), 538 (9.30 × 10<sup>3</sup>), 507 (8.96 × 10<sup>4</sup>), 411 (8.29 × 10<sup>4</sup>). <sup>1</sup>H NMR (pyridine-*d*<sub>5</sub>, 400 MHz): δ 10.20 (d, *J* = 9.6, 1H, meso-H), 9.94 (s, 1H, meso-H), 9.60 (d, *J* = 8.8, 1H, meso-H), 8.80 (s, 1H, CONH), 8.08 (s, 1H, ArH), 7.75 (d, *J* = 7.6, 1H, ArH), 7.51 (d, *J* = 6.8, 1H, ArH), 7.12 (t, *J* = 7.4, 1H, ArH), 6.23 (t, *J* = 6.8, 1H, Gal-H), 5.92 (t, *J* = 8.6, 1H, 3<sup>1</sup>-H), 5.36 (d, *J* = 20.0, 1H, 13<sup>2</sup>-CH<sub>2</sub>), 5.16 (d, *J* = 20.0, 1H, 13<sup>2</sup>-CH<sub>2</sub>), 4.70–4.90 (m, 6H, OCH<sub>2</sub>Ar, Gal-OH), 4.54 (d, *J* = 7.2, 2H, Gal-H), 4.47 (brs, 1H, 18-H), 4.37 (brs, 3H, Gal-H), 4.14 (m, 2H, 17-H and Gal-H), 3.79 (d, *J* = 7.2, 2H, 8-CH<sub>2</sub>CH<sub>3</sub>), 3.74 (s, 3H, ring CH<sub>3</sub>), 3.42 (s, 3H, ring CH<sub>3</sub>), 3.29 (s, 3H, ring CH<sub>3</sub>), 2.90–3.00 (m, 1H, 17<sup>1</sup>-H), 2.60–2.80 (m, 2H, 17<sup>1</sup>-H and 17<sup>2</sup>-H), 2.35–2.45 (m, 1H, 17<sup>2</sup>-H), 2.28 (d, *J* = 5.6, 3H, 3<sup>1</sup>-CH<sub>3</sub>), 1.82 (d, *J* = 6.4, 3H, 18-CH<sub>3</sub>), 1.73 (t, *J* = 6.8, 3H, 8-CH<sub>2</sub>CH<sub>3</sub>), 0.71 (brs, 1H, NH), -1.46 (brs, 1H, NH). HRMS for C<sub>46</sub>H<sub>52</sub>N<sub>5</sub>O<sub>8</sub>I: 929.2862 (calculated); 930.2806 (found, MH<sup>+</sup>).

**Synthesis of 3-[1'-(*m*-Trimethylstannylbenzyloxy)ethyl]-17<sup>2</sup>-(1-amino-1-deoxy)tetraacetogalactosamidepyropheophorbide-a (10).** The title compound was synthesized by following the procedure described for **6** from the respective starting material **7**. Yield: 55%. <sup>1</sup>H NMR (CDCl<sub>3</sub>, 400 MHz): δ 9.77 (s, 1H, meso-H), 9.52 (s, 1H, meso-H), 8.54 (s, 1H, meso-H), 7.43 (m, 2H, ArH), 7.35 (m, 2H, ArH), 5.95–6.05 (m, 2H, CONH and 3<sup>1</sup>-H), 5.37 (d, *J* = 3.2, 1H, Gal-H), 5.26 (d, *J* = 18.8, 1H, 13<sup>2</sup>-CH<sub>2</sub>), 5.18 (d, *J* = 18.8, 1H, 13<sup>2</sup>-CH<sub>2</sub>), 5.02–5.10 (m, 2H, Gal-H), 4.90–5.00 (m, 1H, Gal-H), 4.78 (dd, *J* = 5.8, 11.4, 1H, Gal-H), 4.61 (d, *J* = 11.6, 1H, Gal-H), 4.48 (q, *J* = 7.6, 1H, H-18), 4.36 (m, 1H, H-17), 4.00–4.10 (m, 2H, OCH<sub>2</sub>Ar), 3.95–4.00 (m, 1H, Gal-H), 3.70 (q, *J* = 7.6, 2H, 8-CH<sub>2</sub>CH<sub>3</sub>), 3.66 (s, 3H, ring CH<sub>3</sub>), 3.37 (splits, 3H, ring CH<sub>3</sub>), 3.17 (s, 3H, ring CH<sub>3</sub>), 2.60–2.75 (m, 1H, 17<sup>1</sup>-H), 2.30–2.45 (m, 2H, 17<sup>2</sup>-H and 17<sup>1</sup>-H), 2.12–2.18 (m, 4H, 17<sup>2</sup>-H and 3<sup>1</sup>-CH<sub>3</sub>), 2.04 (s, 3H, COCH<sub>3</sub>), 1.98 (s, 3H, COCH<sub>3</sub>), 1.93 (s, 3H, COCH<sub>3</sub>), 1.90 (s, 3H, COCH<sub>3</sub>), 1.81 (d, *J* = 7.2, 3H, 18-CH<sub>3</sub>), 1.70 (t, *J* = 7.6,

3H, 8-CH<sub>2</sub>CH<sub>3</sub>), 0.45 (brs, 1H, NH), 0.19 (s, 9H, Sn(CH<sub>3</sub>)<sub>3</sub>), -1.69 (brs, 1H, NH). HRMS for C<sub>57</sub>H<sub>69</sub>N<sub>5</sub>O<sub>12</sub>Sn: 1135.3964 (calculated); 1136.3786 (found, MH<sup>+</sup>).

**Synthesis of 3-Devinyl-3-[1'-(*m*-trimethylstannylbenzyloxy)ethyl]-17<sup>2</sup>-(1-amino-1-deoxy)galactosamidepyropheophorbide-a (11).** The title compound was synthesized by following the procedure described for **3** by using the respective starting material **10**. Yield: 55%. Analytical RP HPLC (95/5 MeOH/H<sub>2</sub>O, Symmetry): *t*<sub>R</sub> = 9.88 min, >96%. UV-visible (CH<sub>2</sub>Cl<sub>2</sub>): 661 (4.75 × 10<sup>4</sup>), 605 (8.92 × 10<sup>3</sup>), 537 (9.42 × 10<sup>3</sup>), 505 (9.16 × 10<sup>4</sup>), 408 (8.33 × 10<sup>4</sup>). <sup>1</sup>H NMR (pyridine-*d*<sub>5</sub>, 400 MHz): δ 10.24 (d, *J* = 9.6, 1H, meso-H), 9.95 (s, 1H, meso-H), 9.58 (d, *J* = 9.2, 1H, meso-H), 8.81 (d, *J* = 3.2, 1H, CONH), 7.77 (s, 1H, ArH), 7.66 (m, 1H, ArH), 7.60 (m, 1H, ArH), 7.51 (m, 1H, ArH), 6.28 (m, 1H, Gal-H), 5.92 (t, *J* = 8.8, 1H, 3<sup>1</sup>-H), 5.36 (d, *J* = 20.0, 1H, 13<sup>2</sup>-CH<sub>2</sub>), 5.16 (d, *J* = 20.4, 1H, 13<sup>2</sup>-CH<sub>2</sub>), 5.00 (d, *J* = 11.6, 1H, Gal-H), 4.84 (brs, 5H, Gal-H and Gal-OH), 4.54 (m, 2H, Gal-H), 4.47 (m, 1H, 18-H), 4.37 (m, 3H, OCH<sub>2</sub>Ar and Gal-H), 4.14 (m, 2H, 17-H, Gal-H), 3.79 (d, *J* = 7.6, 2H, 8-CH<sub>2</sub>CH<sub>3</sub>), 3.75 (s, 3H, ring CH<sub>3</sub>), 3.44 (splits, 3H, ring CH<sub>3</sub>), 3.24 (s, 3H, ring CH<sub>3</sub>), 2.90–3.00 (m, 1H, 17<sup>1</sup>-H), 2.60–2.80 (m, 2H, 17<sup>2</sup>-H and 17<sup>1</sup>-H), 2.35–2.45 (m, 1H, 17<sup>2</sup>-H), 2.29 (d, *J* = 6.0, 3H, 3<sup>1</sup>-CH<sub>3</sub>), 1.82 (d, *J* = 6.8, 3H, 18-CH<sub>3</sub>), 1.73 (t, *J* = 7.4, 3H, 8-CH<sub>2</sub>CH<sub>3</sub>), 0.75 (brs, 1H, NH), 0.23 (s, 9H, Sn(CH<sub>3</sub>)<sub>3</sub>), -1.42 (d, *J* = 5.6, 1H, NH). HRMS for C<sub>49</sub>H<sub>61</sub>N<sub>5</sub>O<sub>8</sub>Sn: 967.3541 (calculated): 968.3452 (found, MH<sup>+</sup>).

**Radioactive Labeling.** <sup>124</sup>I-Analogues of **2** and **3** were prepared from the corresponding trimethylstannyl analogues **9** and **11**, respectively, by following the procedure as described below for <sup>124</sup>I analogue of compound **1**.

**Synthesis of <sup>124</sup>I-Analogue of 3-[1'-(*m*-Iodobenzyloxy)ethyl]-pyropheophorbide-a Methyl Ester (1).** The trimethyltin analogue **12** (50 μg) was dissolved in 50 μL of 5% acetic acid in methanol. Then 100 μL of 5% acetic acid in methanol was added to Na<sup>124</sup>I in 10 μL of 0.1 N NaOH. The two solutions were mixed, and an IODOGEN bead (Pierce Biotechnology, Inc., Rockford, IL 61106) was added. The reaction mixture was incubated at room temperature for 15 min, iodobead was removed, and the reaction mixture was injected on an HPLC column (Phenomenex Maxsil C8 5 μm), which was eluted with an isocratic 90/10 MeOH/H<sub>2</sub>O at a flow rate of 1 mL/min. The UV detector was set at 254 nm wavelength. The labeled product (**1**) that eluted at 10.53 min (Supporting Information) was collected, and the solvent was evaporated to dryness under a stream of N<sub>2</sub> at 60 °C. The product was formulated in saline containing 10% ethanol for in vivo experiments. RadioTLC confirmed the radiochemical purity (>95%) of the product. A standard curve was generated between peak area versus mass by injecting a known mass of carrier **1** onto the column. The mass associated with the labeled product was calculated by relating the peak area of UV absorbance peak of **1** in the labeled product to the standard curve. The specific activity was obtained by dividing the activity of the labeled product collected by the calculated mass in micromoles. Specific activity of radiolabeled product for five runs was in the range 2.1 ± 1.4 (9) Ci/μmol. The radiochemical yield of the reaction was 20%.

**HPLC conditions for compound 2:** eluant, MeOH/water, 95:5; wavelength, 254 nm; flow rate, 1 mL/min; retention time for the <sup>124</sup>I-derivative, 9 min; retention time for the intermediate trimethyl tin derivative, 11 min; column, Symmetry, C18; radiochemical yield, 36%; specific activity, 4.3 Ci/μmol.

**HPLC conditions for compound 3:** eluant, MeOH/water, 95:10; wavelength, 254 nm; flow rate, 1 mL/min; retention time for the <sup>124</sup>I-derivative, 22.8 min; retention time for the intermediate trimethyl tin derivative, 27.8 min; column, Maxsil; radiochemical yield, 14%; specific activity, 3.2 Ci/μmol.

**In Vivo Photosensitizing Efficacy (Kaplan–Meier Plot).** The female C3H/HeJ mice were intradermally injected with 2 × 10<sup>5</sup> RIF cells in 30 μL of HBSS without Ca<sup>2+</sup> and Mg<sup>2+</sup> on the flank, and tumors were grown until they reached 4–5 mm in diameter. The day before laser light treatment, all hair was removed from the inoculation site and the mice were injected intravenously with varying photosensitizers' doses. At 24 h postinjection, the

mice were restrained without anesthesia in plastic holders and then treated with laser light from a dye laser tuned to emit drug-activating wavelengths. The treatment parameters consisted of an irradiated area of 1 cm<sup>2</sup>, a fluence rate of 75 mW/cm<sup>2</sup> for a dose of 135 J/cm<sup>2</sup>. The mice were observed daily for signs of weight loss, necrotic scabbing, or tumor regrowth. If tumor growth appeared, and the tumors were measured using two orthogonal measurements *L* and *W* (perpendicular to *L*), and the volumes were calculated using the formula  $V = (L \times W^2)/2$  and recorded. Mice were considered cured if there was no sign of tumor regrowth by day 60 after PDT treatment.

**PET Imaging.** Mice were imaged in the microPET FOCUS 120, a dedicated 3D small-animal PET scanner (Concorde Microsystems Incorporated) at State University of New York at Buffalo under the Institutional Animal Care and Use Committee (IACUC) guidelines. The C3H mice were subcutaneously injected with  $3 \times 10^5$  RIF cells in 30  $\mu$ L of complete  $\alpha$ -MEM (into the axilla), and tumors were grown until they reached 4–5 mm in diameter (approximately 5 days). All tumored C<sub>3</sub>H mice were injected via the tail vein with 72–200  $\mu$ Ci of **1–3** and after 24, 48, 72, and 96 h postinjection the mice were anesthetized by inhalation of isoflurane/oxygen, placed head first prone for imaging, and the acquisition time was set for 30 min. Radioiodine uptake by thyroid or stomach was not blocked. All mice going through imaging were marked with a cross-line on the back to provide a reference landmark for consistently positioning them in a series of imaging studies. The acquired data were rebinned with FORE algorithm<sup>20</sup> and reconstructed with 2D OSEM algorithm. The dead-time and singles-based random coincidence corrections were applied to all the PET studies. The RUV results were calculated from PET images with attenuation and scatter corrections, in addition to the dead-time and random coincidence corrections. The transmission scan for attenuation correction was carried out with a rotating <sup>57</sup>Co point source.

**Biodistribution Studies.  $\gamma$  Well Counter.** All studies were performed as per IACUC guidelines. The mice (three to four mice for each compound per time point) were injected with 15–200  $\mu$ Ci of **1–3** via tail vein and were sacrificed at 24, 48, 72, and 96 h postinjection, blood and body organs (tumor, heart, liver, spleen, kidney, lung, muscle, gut, and stomach) being removed immediately. After the samples were weighed, the amount of radioactivity in the tumor (50–150 mg), body organs, and blood was measured by a  $\gamma$  well counter. Radioactivity uptake was calculated as the percentage of the injected dose per gram of the tissue (% ID/g). Statistical analyses and data (% ID/g vs time point) were plotted using Microsoft Excel.

**Acknowledgment.** Financial support from the NIH (Grants CA 114053, CA127369, and CA55791), Roswell Park Alliance Foundation, and the shared resources of the RPCI (Support Grant P30CA16056) is highly appreciated.

**Supporting Information Available:** <sup>1</sup>H NMR spectra for compounds **1–3**, **6**, **9**, **10**, and **12** and the analytical details of compounds **1–12**. This material is available free of charge via the Internet at <http://pubs.acs.org>.

## References

- Massoud, T. F.; Gambhir, S. S. Molecular imaging in living subjects: seeing fundamental biological processes in a new light. *Genes Dev.* **2003**, *17*, 545–580.
- Gambhir, S. S.; Czernin, J.; Schwimmer, J.; Silverman, D. H. S.; Coleman, R. E.; Phelps, M. E. A tabulated summary of the FDG PET literature. *J. Nucl. Med.* **2001**, *42* (Suppl.), 1S–93S.
- Abouzed, M. M.; Crawford, E. S.; Nabi, H. A. 18F-FDG imaging: pitfalls and artifacts. *J. Nucl. Med. Technol.* **2005**, *33*, 145–155.
- (a) Pentlow, K. S.; Graham, M. C.; Lambrecht, R. M.; Daghighian, F.; Bacharach, S. L.; Bendriem, B.; Finn, R. D.; Jordon, K.; Kalaigian, H.; Karp, J. S.; Robeson, W. R.; Larson, S. M. Quantitative imaging of iodine-124 with PET. *J. Nucl. Med.* **1996**, *37*, 1557–1562. (b) Trotter, D. E. G.; Manjeshwar, R. M.; Doss, M.; Shaller, C.; Robinson, M. K.; Tandon, R.; Adams, G. P.; Adler, L. P. Quantitation of small-animal <sup>124</sup>I-activity distributions using a clinical PET/CT scanner. *J. Nucl. Med.* **2004**, *45*, 1237–1244.
- (a) Verel, I.; Visser, G. W. M.; vanDongen, G. A. M. S. The promise of immuno-PET in radioimmunotherapy. *J. Nucl. Med.* **2005**, *46*, 164S–171S. (b) Bennett, J. J.; Tjuvajev, J.; Johnson, P.; Doubrovina, M.; Akhurst, T.; Malholtra, S.; Hackman, T.; Balatoni, J.; Finn, R.; Larson, S. M.; Federoff, H.; Blasberg, R.; Fong, Y. M. Positron emission tomography imaging for herpes virus infection: implications for oncolytic viral treatments of cancer. *Nat. Med.* **2001**, *7*, 859–863. (c) Doubrovina, M.; Ponomarev, V.; Beresten, T.; Balatoni, J.; Bornmann, W.; Finn, R.; Humm, J.; Larson, S.; Sadelain, M.; Blasberg, R.; Tjuvajev, J. G. Imaging transcriptional regulation of p53-dependent genes with positron emission tomography in vivo. *Proc. Natl. Acad. Sci. U.S.A.* **2001**, *98*, 9300–9305. (d) Jacobs, A.; Voges, J.; Reszka, R.; Lercher, M.; Gossmann, A.; Kracht, L.; Kaestle, C.; Wagner, R.; Wienhard, K.; Heiss, W. D. Positron-emission tomography of vector-mediated gene expression in gene therapy for gliomas. *Lancet* **2001**, *358*, 727–729. (e) Divgi, C. R.; Pandit-Taskar, N.; Jungbluth, A. A.; Reuter, V. E.; Gonen, M.; Ruan, S.; Pierre, C.; Nagel, A.; Pryma, D. A.; Humm, J.; Larson, S. M.; Old, L. J.; Russo, P. Preoperative characterization of clear-cell renal carcinoma using iodine-124 labelled antibody chimeric G250 (124I-cG250) and PET in patients with renal masses: a phase I trial. *Lancet Oncol.* **2007**, *8*, 304–310.
- (a) Henderson, B. W.; Dougherty, T. J. How does photodynamic therapy work? *Photochem. Photobiol.* **1992**, *55*, 145–157. (b) Dougherty, T. J.; Gomer, C. J.; Henderson, B. W.; Jori, G.; Kessel, D.; Korbelik, M.; Moan, J.; Peng, Q. Photodynamic therapy. *J. Natl. Cancer. Inst.* **1998**, *90*, 889–905.
- Dolmans, D. E.; Fukumura, D.; Jain, R. K. Photodynamic therapy for cancer. *Nat. Rev. Cancer* **2003**, *3*, 380–387.
- (a) Pandey, R. K.; Sumlin, A. B.; Constantine, S.; Aoudia, M.; Potter, W. R.; Bellnier, D. A.; Henderson, B. W.; Rodgers, M. A.; Smith, K. M.; Dougherty, T. J. Alkyl ether analogs of chlorophyll-*a* derivatives: part 1. Synthesis, photophysical properties and photodynamic efficacy. *Photochem. Photobiol.* **1996**, *64*, 194–204. (b) Henderson, B. W.; Bellnier, D. A.; Greco, W. R.; Sharma, A.; Pandey, R. K.; Vaughan, L. A.; Weishaupt, K. R.; Dougherty, T. J. An in vivo quantitative structure–activity relationship for a congeneric series of pyropheophorbide derivatives as photosensitizers for photodynamic therapy. *Cancer Res.* **1997**, *57*, 4000–4007. (c) Dougherty, T. J.; Sumlin, A. B.; Greco, W. R.; Weishaupt, K. R.; Vaughan, L. A.; Pandey, R. K. The role of the peripheral benzodiazepine receptor in photodynamic activity of certain pyropheophorbide ether photosensitizers: albumin site II as a surrogate marker for activity. *Photochem. Photobiol.* **2002**, *76*, 91–97. (d) Bellnier, D. A.; Greco, W. R.; Loewen, G. M.; Bellnier, D. A.; Nava, H.; Oseroff, A. R.; Pandey, R. K.; Tsuchida, T.; Dougherty, T. J. Population pharmacokinetics of the photodynamic therapy agent 2-[1-hexyloxyethyl]-2-devinyl pyropheophorbide-*a* in cancer patients. *Cancer Res.* **2003**, *63*, 1806–1813. (e) Bellnier, D. A.; Greco, W. R.; Nava, H.; Loewen, G. M.; Oseroff, A. R.; Dougherty, T. J. Mild skin photosensitivity in cancer patients following injection of photochlor [2-(1'-hexyloxyethyl)-2-devinyl pyropheophorbide-*a*; HPPH] for photodynamic therapy. *Cancer Chemother. Pharmacol.* **2006**, *57*, 40–45.
- (a) Westermann, P.; Glanzmann, T.; Andrejevic, S.; Braichotte, D. R.; Forrer, M.; Wagnieres, G. A.; Monnier, P.; Van, D. B. H.; Mach, J. P.; Folli, S. Long circulating half-life and high tumor selectivity of the photosensitizer meta-tetrahydroxyphenylchlorin conjugated to polyethylene glycol in nude mice grafted with a human colon carcinoma. *Int. J. Cancer* **1998**, *76*, 842–850. (b) Vrouenraets, M. B.; Visser, G. W. M.; Stewart, F. A.; Vrouenraets, M. B.; Visser, G. W. M.; Stewart, F. A.; Stigter, M.; Oppelaar, H.; Postmus, P. E.; Snow, G. B.; van Dongen, G. A. M. S. Development of meta-tetrahydroxyphenylchlorin-monooclonal antibody conjugates for photodynamic therapy. *Cancer Res.* **1999**, *59*, 1505–1513. (c) Whelpton, R.; Michael-Titus, A. T.; Jamdar, R. P.; Abdillahi, K.; Grahn, M. F. Distribution and excretion of radiolabeled temoporfin in a murine tumor model. *Photochem. Photobiol.* **1996**, *63*, 885–891. (d) Wilson, B. C.; VanLier, J. E. Radiolabelled photosensitizers for tumor imaging and photodynamic therapy. *J. Photochem. Photobiol., B* **1989**, *3*, 459–463.
- (a) Chen, Y.; Gryshuk, A.; Achilefu, S.; Ohulchansky, T.; Potter, W.; Zhong, T. X.; Morgan, J.; Chance, B.; Prasad, P. N.; Henderson, B. W.; Oseroff, A.; Pandey, R. K. A novel approach to a bifunctional photosensitizer for tumor imaging and phototherapy. *Bioconjugate Chem.* **2005**, *16*, 1264–1274. (b) Pandey, S. K.; Chen, Y.; Zawada, R. H.; Oseroff, A.; Pandey, R. K. Utility of tumor-avid photosensitizers in developing bifunctional agents for tumor imaging and/or phototherapy. *Proc. SPIE* **2006**, *6139*, 613905/1–613905/7.

- (11) Ma, B.; Li, G.; Kanter, P.; Lamonica, D.; Grossman, Z.; Pandey, R. K. Bifunctional HPPH-N<sub>2</sub>S<sub>2</sub> Tc-99m conjugates as tumor imaging agents: synthesis and biodistribution studies. *J. Porphyrins Phthalocyanines* **2003**, *1*, 500–507.
- (12) Pandey, S. K.; Gryshuk, A. L.; Sajjad, M.; Zheng, X.; Chen, Y.; Abouzeid, M. M.; Morgan, J.; Charamisinau, I.; Nabi, H. A.; Oseroff, A.; Pandey, R. K. Multimodality agents for tumor imaging (PET, fluorescence) and photodynamic therapy. A possible “see and treat” approach. *J. Med. Chem.* **2005**, *48*, 6286–6294.
- (13) (a) Zheng, G.; Graham, A.; Shibata, M.; Missert, J. R.; Oseroff, A. R.; Dougherty, T. J.; Pandey, R. K. Synthesis of beta-galactose-conjugated chlorins derived by enyne metathesis as galectin-specific photosensitizers for photodynamic therapy. *J. Org. Chem.* **2001**, *66*, 8709–8716. (b) Li, G.; Pandey, S. K.; Graham, A.; Dobhal, M. P.; Mehta, R.; Chen, Y. H.; Gryshuk, A.; Rittenhouse-Olson, K.; Oseroff, A.; Pandey, R. K. Functionalization of OEP-based benzochlorins to develop carbohydrate-conjugated photosensitizers. Attempt to target beta-galactoside-recognized proteins. *J. Org. Chem.* **2004**, *69*, 158–172. (c) Pandey, S. K.; Zheng, X.; Morgan, J.; Missert, J. R.; Liu, T. H.; Shibata, M.; Bellnier, D. A.; Oseroff, A. R.; Henderson, B. W.; Dougherty, T. J.; Pandey, R. K. Purpurinimide carbohydrate conjugates: effect of the position of the carbohydrate moiety in photosensitizing efficacy. *Mol. Pharmaceutics* **2007**, *4*, 448–464. (d) Haubner, R.; Kuhnast, B.; Mang, C.; Weber, W. A.; Kessler, H.; Wester, H. J.; Schwaiger, M. <sup>18</sup>F-Galacto-RGD: synthesis, radiolabeling, metabolic stability, and radiation dose estimates. *Bioconjugate Chem.* **2004**, *15*, 61–69.
- (14) Speizer, L.; Haugland, R.; Kutchai, H. Asymmetric transport of a fluorescent glucose analogue by human erythrocytes. *Biochem. Biophys. Acta* **1985**, *815*, 75–84.
- (15) Zhang, M.; Zhang, Z.; Blessington, D.; Li, H.; Busch, T. M.; Madrak, V.; Miles, J.; Chance, B.; Glickson, J. D.; Zheng, G. Pyropheophorbide 2-deoxyglucosamide: a new photosensitizer targeting glucose transporters. *Bioconjugate Chem.* **2003**, *14*, 709–714.
- (16) Zheng, X.; Pandey, R. K.; et al. Unpublished results.
- (17) Zheng, G.; Potter, W. R.; Camacho, S. H.; Missert, J. R.; Wang, G. S.; Bellnier, D. A.; Henderson, B. W.; Rodgers, M. A. J.; Dougherty, T. J.; Pandey, R. K. Synthesis, photophysical properties, tumor uptake, and preliminary in vivo photosensitizing efficacy of a homologous series of 3-(1'-alkyloxy)ethyl-3'-devinylpurpurin-18-N-alkylimides with variable lipophilicity. *J. Med. Chem.* **2001**, *44*, 1540–1559.
- (18) Smith, K. M.; Golf, D. A.; Simpson, D. A. Meso substitution of chlorophyll derivatives: direct route for transformation of bacteriopheophorbides *d* into bacteriopheophorbides *c*. *J. Am. Chem. Soc.* **1985**, *107*, 4941–4954.
- (19) Sajjad, M.; Bars, E.; Nabi, H. A. Optimization of <sup>124</sup>I production via <sup>124</sup>Te(p,n)<sup>124</sup>I reaction. *App. Radiat. Isot.* **2006**, *64*, 965–970.
- (20) Defrise, M.; Kinahan, P. E.; Townsend, D. W.; Michel, C.; Sibomana, M.; Newport, D. F. Exact and approximate rebinding algorithms for 3-D PET data. *IEEE Trans. Med. Imaging* **1997**, *16* (2), 145–158.

JM8012213